IOPscience iopscience.iop.org

Home Search Collections Journals About Contact us My IOPscience

Characteristics of global energy confinement in KSTAR L- and H-mode plasmas

This content has been downloaded from IOPscience. Please scroll down to see the full text.

2014 Nucl. Fusion 54 083012

(http://iopscience.iop.org/0029-5515/54/8/083012)

View the table of contents for this issue, or go to the journal homepage for more

Download details:

IP Address: 198.125.229.230
This content was downloaded on 27/06/2014 at 15:46

Please note that terms and conditions apply.

IOP Publishing | International Atomic Energy Agency Nuclear Fusion
Nucl. Fusion **54** (2014) 083012 (11pp) doi:10.1088/0029-5515/54/8/083012

Characteristics of global energy confinement in KSTAR L- and H-mode plasmas

H.-S. Kim[1], Y.M. Jeon[2], Y.-S. Na[1], Y.-c. Ghim[3], J.-W. Ahn[4], S.W. Yoon[2], J.G. Bak[2], Y.S. Bae[2], J.S. Kim[2], M. Joung[2], J.-H. Jeong[2], S.H. Hong[2], K.M. Kim[5], T. Suzuki[6], W.C. Kim[7], J.-G. Kwak[2] and The KSTAR Team

[1] Department of Nuclear Engineering, Seoul National University, Seoul, Korea
[2] National Fusion Research Institute, Daejeon, Korea
[3] Department of Nuclear and Quantum Engineering, KAIST, Daejeon, Korea
[4] Oak Ridge National Laboratory, Oak Ridge, TN, USA
[5] Princeton Plasma Physics Laboratory, Princeton, NJ, USA
[6] Japan Atomic Energy Agency, Naka, Japan
[7] ITER Organization, Saint-Paul-Lez-Durance, France

E-mail: ysna@snu.ac.kr

Received 13 November 2013, revised 26 March 2014
Accepted for publication 2 May 2014
Published 11 June 2014

Abstract

We evaluate the characteristics of global energy confinement in KSTAR ($\tau_{E,KSTAR}$) quantitatively in three ways; firstly by comparing it with multi-machine scalings, secondly by deriving multiple regression equations for the L- and the H-mode plasmas, respectively, and lastly by comparing confinement enhancement of the H-mode phase with respect to the L-mode phase in each discharge defined as H_{exp}. The KSTAR database exhibits $\tau_{E,KSTAR}$ of ~0.04 to ~0.16 s and of ~0.06 to ~0.19 s in L-mode and in H-mode plasmas, respectively. The multiple regression equations derived by statistical analysis present the similar dependency on P_L and higher dependency on I_p compared with the multi-machine scalings, however the dependency on κ in both L- and H-mode plasmas draw the negative power dependency of $\kappa^{-0.68}$ and $\kappa^{-0.76}$ for H-mode and for L-mode database, respectively on the contrary to the positive dependency in all multi-machine empirical scalings. It is found that the energy confinement of both L-mode and H-mode of the discharges with $H_{exp} > 1.5$ can be well-predicted by multi-machine scalings, $\tau_{E,89L}$ and $\tau_{E,92H}$. Apart from this, the H-mode confinement with $1.5 < H_{exp} < 2.0$ is well-predicted by using the multi-machine empirical L-mode scaling $\tau_{E,89L}$.

Keywords: KSTAR, global energy confinement time, multi-machine scaling, confinement enhancement, L-mode, H-mode, regression analysis

(Some figures may appear in colour only in the online journal)

1. Introduction

Deriving empirical scalings for global energy confinement time is extremely important in designing and extrapolating plasma performance of a next-step tokamak and a fusion reactor since a dependency of energy transport on plasma parameters has not been fully understood yet. A variety of empirical scalings of the energy confinement time in both L-mode and H-mode operating regimes have been derived since around 1980s. For the global energy confinement scalings, historically, Kaye *et al* initiated the activity by building the international L-mode confinement database [1–3] and deriving the multi-machine L-mode scalings. The initial multi-machine H-mode confinement database (ITERH.DB2) assembled by the H-mode database working group was used to extract empirical scalings exhibiting the H-mode confinement [4–8] with contributions from six machines (ASDEX, DIII-D, JET, JFT-2 M, PBX-M, and PDX). In sequence, the database has been improved (ITERH.DB3) by including experimental data from additional tokamaks (ASDEX Upgrade, COMPASS-D, TCV, TEXTOR, JT-60U, and Alcator C-Mod) so that improved empirical scalings of the H-mode confinement have been drawn [9, 10]. The multi-machine scalings derived from ITERH.DB2 and ITERH.DB3 deal with the global energy confinement as well as the thermal energy confinement in both edge localized mode (ELM)-free and ELMy H-mode

 © 2014 IAEA, Vienna Printed in the UK

Table 1. Range of main parameters of database used for confinement studies in KSTAR.

	In database, H-mode phase	L-mode phase	Unit	Measurement error
Plasma current (I_P)	0.40–0.90	0.40–0.76	MA	$\leqslant$0.7%
Toroidal magnetic field (B_T)	1.3–3.0	1.5–3.0	T	$\leqslant$0.1%
Line averaged electron density ($\bar{n}_e$)	1.63–6.03	0.43–3.22	$10^{19}\,m^{-3}$	$\leqslant 0.03 \times 10^{19}\,m^{-3}$
Major radius (R)	1.78–1.92	1.76–1.87	m	Real time EFIT
Minor radius (a)	0.43–0.51	0.44–0.51	m	Real time EFIT
Elongation (κ)	1.55–2.06	1.65–1.93		Real time EFIT
NBI heating power (P_{NBI})	1.10–3.50	1.10–3.50	MW	$\leqslant$3.0%
EC heating power (P_{EC})	0.0–0.35	0.0–0.25	MW	$\leqslant$5.0%
Diamagnetic stored energy (W_{dia})	0.15–0.50	0.09–0.28	MJ	$\leqslant$5.0%

discharges. Apart from evaluating the energy confinement by scalings based on database, energy confinement of the H-mode phase can be evaluated in each discharge by H_{exp} which describes how much plasma confinement is enhanced in the H-mode phase relative to the L-mode phase in a single discharge [11–13].

Before evaluating the characteristics of the global energy confinement of KSTAR (Korea Superconducting Tokamak Advanced Research) compared with the multi-machine scalings, KSTAR experiment is summarized. KSTAR is aiming at long-pulse high performance plasma operations with fully superconducting magnets [14, 15], which are one of the most important tasks that must be sorted out in order to commercialize the fusion energy. Since KSTAR has been operating from the year 2008 and obtained the first H-mode discharge in the year 2010 [16], ELMy H-mode discharges have been routinely produced up to now by utilizing combined auxiliary heating of neutral beam injection (NBI) and electron cyclotron resonant heating (ECRH). Most of H-mode discharges in KSTAR are sustained for more than ~5 s up to ~20 s with the central electron and ion temperature of $T_{e0} \sim T_{i0} \sim$ 2–3 keV and the central toroidal rotation of ~200–250 km s^{-1} when with full injection of NBI power of 3 MW. The stability-relevant parameters, normalized beta β_N and internal inductance l_i, reach the range of $\beta_N \leqslant 3.0$ and $l_i \geqslant 0.7$, respectively [17]. In addition, sawtooth-free regimes with $q(0)$ above unity have been achieved recently so that KSTAR begins to address advanced tokamak physics issues [18]. Various wall-cleaning techniques have been used in order to optimize the wall conditions and minimize the radiation power loss from the impurities in KSTAR. They are listed up as high temperature baking up to 250 °C for the PFCs, overnight He glow discharge cleaning (GDC), and boronization with carborane [16].

The purpose of this work is to calculate and evaluate the global energy confinement time of the KSTAR L- and the H-mode regime in a quantitative way by collecting all of the KSTAR discharges for 2 years for completeness of previous studies [16]. Here we employ three approaches to evaluate the characteristics of the KSTAR confinement. One is comparing with the multi-machine scalings. Another is newly deriving multiple regression equations for KSTAR and comparing them with the multi-machine scalings. The other is analyzing the confinement enhancement in each discharge in terms of H_{exp}.

The paper is organized as follows. Section 2 describes the details of calculation of the global energy confinement time in KSTAR ($\tau_{E,KSTAR}$). In section 3, the characteristic of $\tau_{E,KSTAR}$ in the L-mode phase as well as the H-mode phase is discussed not only by comparing with multi-machine scalings but also by producing its own scaling of KSTAR using the multiple regression analysis. In section 4, the confinement enhancement factor is calculated in each discharge and the characteristics of KSTAR energy confinement are discussed. Section 5 is devoted to conclude our work.

2. Calculation of global energy confinement of L- and H-mode plasmas in KSTAR

2.1. Criteria on building database for KSTAR discharges

The selection criteria of the standard dataset for multi-machine scalings [7] are (1) Omit high radiation discharges, $P_{rad}/P_T \leqslant 0.6$, where $P_T = P_{aux} + P_{ohm}$, (2) Limit the fast ion content, $W_{fast\ ion}/W \leqslant 0.40$, (3) Omit discharges with degraded confinement due to sawtooth and beam deposition effects, (4) Omit transient discharges, $-0.05 \leqslant W/P_T \leqslant 0.35$, and (5) Omit discharges with excessive MHD activity near a beta limit. We try to sort out the discharges about 250 L- and H-mode discharges selected in the 4th (year 2011) and 5th (year 2012) campaign of KSTAR experiment in accordance with the selection criteria of the multi-machine database so to build a KSTAR database to analyze $\tau_{E,KSTAR}$. Table 1 presents the range of main parameters in the database built on the basis of these selection criteria. It describes the conditions operated routinely in KSTAR. The available external heating includes 1.1–3.0 MW of NBI with the beam energy of 60–95 keV for duration of ~20 s and 0.35 MW of ECRH from the 110 GHz gyrotron for ~3 s. The 1.0 MW of ECRH from the 170 GHz gyrotron for duration of ~10 s is not used in the selected discharges of the database. Most of discharges are operated with ~1.8 m of major radius (R), ~0.5 m of minor radius (a), 0.4–0.9 MA of plasma current (I_P), and 1.3–3.0 T of toroidal magnetic field (B_T). The shaping parameters have been achieved in the range of elongation (κ) $\leqslant$ 2.1 and triangularity (δ) $\leqslant$ 0.9. It is noteworthy that R and a in the database present little variation.

Figure 1 represents a typical KSTAR H-mode discharge (#7081) with $I_P = 0.6$ MA, $B_T = 2.0$ T contained in the database established. The H-mode transition begins to occur around 2.6 s where $P_{NBI} = 3.0$ MW, $\bar{n}_e \sim 1.6 \times 10^{19}\,m^{-3}$, and $\kappa \sim 1.7$ with $\tau_{E,KSTAR} \sim 0.06$ s presenting a L-mode confinement. Eventually, it achieves $W_{dia} \sim 0.3$ MJ, $\bar{n}_e \sim 3.2 \times 10^{19}\,m^{-3}$, and $\tau_{E,KSTAR} \sim 0.1$ s when reaching the H-mode phase. For identification of the L–H transition, D_α monitors and W_{dia} measured by diamagnetic loops are utilized.

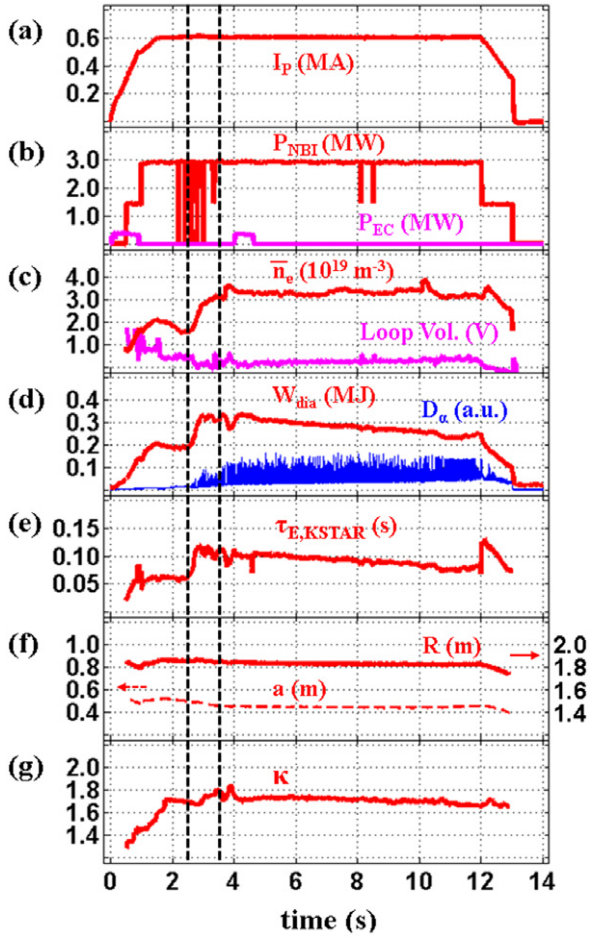

Figure 1. A typical KSTAR H-mode discharge, #7081. (*a*) The plasma current (I_P) in MA, (*b*) the external heating power of NBI (P_{NBI}) and ECRH (P_{EC}) in MW, (*c*) the line averaged electron density ($\bar{n}_e$) in 10^{19} m^{-3} and the loop voltage in *V*, (*d*) the diamagnetic stored energy (W_{dia}) in MJ and the D_α signal in a.u., (*e*) the calculated global energy confinement time ($\tau_{E,KSTAR}$) in s, (*f*) the major radius (*R*) in m and the minor radius (*a*) in m, and (*g*) the plasma elongation (κ).

In order to establish the database for analyzing $\tau_{E,KSTAR}$, we choose two time points in each discharge; one at the L-mode phase and the other at the H-mode phase. These two time points are selected with care. An example is given in figure 1 where the vertical dashed lines represent these selected time points. As shown in figures 1(*d*) and (*e*), the plasma is still in transient state for several hundreds of milliseconds after the L–H transition. Also as shown, KSTAR H-mode discharges exhibit a gradual degradation of W_{dia} and $\tau_{E,KSTAR}$ during the H-mode phase even though the auxiliary heating power is constant. This is because the control of plasma shape and position is not optimized and stabilized yet in the KSTAR discharges. Therefore, for the H-mode phase, the time is selected between 0.5 to 1.0 s after the L–H transition even though dW_{dia}/dt is still somewhat varying. We define $\tau_{E,KSTAR,H}$ as $\tau_{E,KSTAR}$ calculated at this time point where the subscription 'H' represents the data point of a KSTAR H-mode phase. In the case of L-mode, the time is selected right before the L–H transition begins. We define $\tau_{E,KSTAR,L}$ as $\tau_{E,KSTAR}$ calculated at this time point where the subscription 'L' represents the data point of a KSTAR L-mode phase.

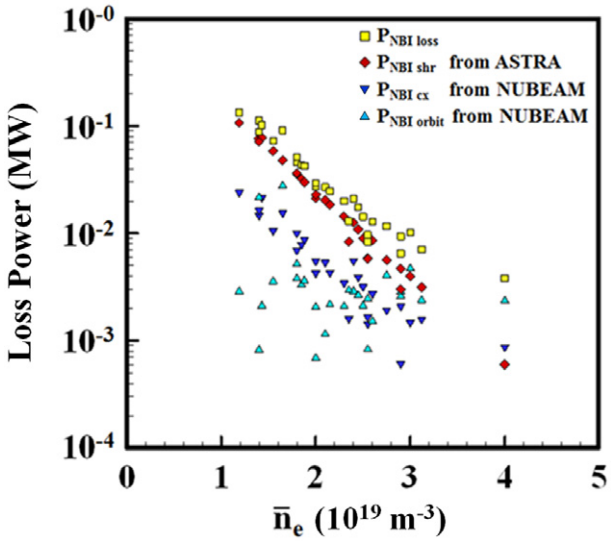

Figure 2. $P_{NBI\ loss}$ (yellow square) due to shine-through (red diamond), charge exchange (inverted blue triangle), and bad ion orbit (sky blue triangle) against density variation for some selected discharges calculated by the NBI module embedded in ASTRA and by NUBEAM.

2.2. Calculation of global energy confinement in KSTAR

We evaluate overall confinement characteristics of KSTAR H-mode discharges in terms of the global energy confinement time (τ_E) and the confinement enhancement factors. As well known in literature, τ_E can be expressed with W_{dia} and P_L. In this work, W_{dia} is the global stored energy determined by diamagnetic loop measurements. The power balance equation adopted to calculate P_L is expressed as follow:

$$\frac{dW_{dia}}{dt} = P_{ohm} + P_{aux} - P_L \qquad (1)$$

It is composed of terms describing the ohmic heating power (P_{ohm}), the delivered auxiliary heating power (P_{aux}) in which NBI and ECRH are main sources, the power loss from the core to the seperatrix (P_L), and the time derivative of the diamagnetic stored energy (dW_{dia}/dt). Here, the analytic time interval (Δt) for dW_{dia}/dt is assumed to be 50 ms.

In the power balance equation, P_{ohm} is calculated by multiplying the surface voltage of the plasma to the plasma current [19]. The surface voltage in KSTAR is obtained directly from the loop voltage diagnostics located on the equatorial plane of the high field side. It is noteworthy that only the resistive component in the total induced voltage has to be considered for calculating P_{ohm}. In the L-mode phase, however some selected points are still in the ramp-up phase of the plasma current so that the inductive component has to be subtracted from the total voltage. Because P_{NBI} is usually fully injected far prior to the selected point of L-mode phase, the contribution of inductive component is not significant in calculating P_L. H-mode database of KSTAR discharges is collected in the flat-top phase where the flux is only consumed by the resistive way [20].

P_{aux} is obtained directly from experiments as a delivered power, not an absorbed one. It is well-known that the absorbed power of heating sources has to be considered to calculate P_L more accurately. At present, the KSTAR is equipped with

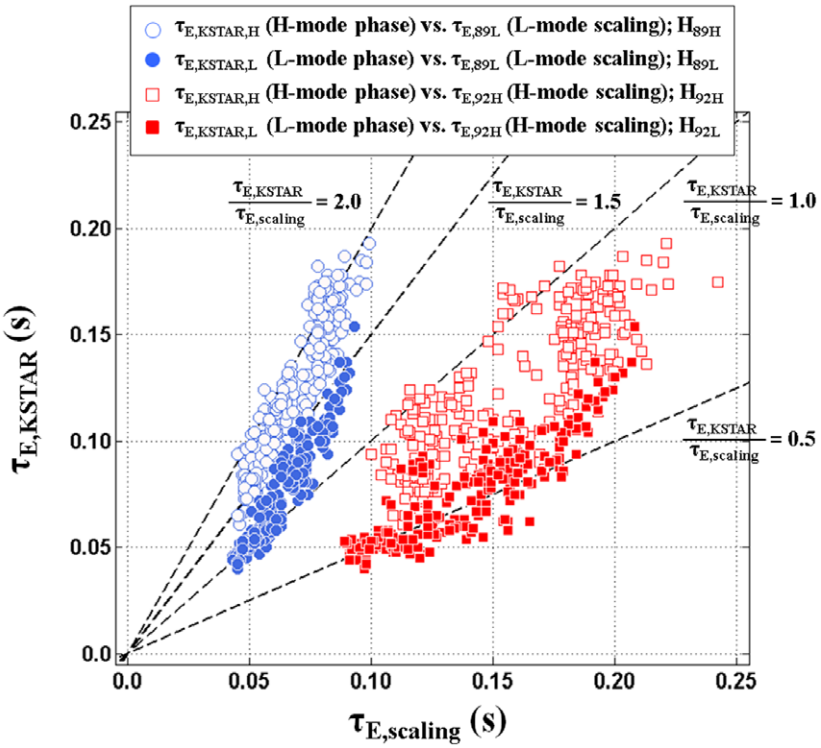

Figure 3. $\tau_{E,KSTAR}$ versus $\tau_{E,scaling}$ ($\tau_{E,89L}$ and $\tau_{E,92H}$) representing H_{89L}, H_{89H}, H_{92L}, and H_{92H}. H_{89H} and H_{92H} are the confinement enhancement factor of 'H-mode database of KSTAR discharges' compared with the L- and H-mode multi-machine scalings, $\tau_{E,89L}$ and $\tau_{E,92H}$, respectively; $H_{89H} = \tau_{E,KSTAR,H}/\tau_{E,89L}$, $H_{92H} = \tau_{E,KSTAR,H}/\tau_{E,92H}$. H_{89L} and H_{92L} are the confinement enhancement factor of 'L-mode database of KSTAR discharges' compared with the multi-machine scalings, $\tau_{E,89L}$ and $\tau_{E,92H}$, respectively; $H_{89L} = \tau_{E,KSTAR,L}/\tau_{E,89L}$, $H_{92L} = \tau_{E,KSTAR,L}/\tau_{E,92H}$. The circle markers and the square markers represent $\tau_{E,KSTAR}$ against the scalings derived from L-mode database ($\tau_{E,89L}$) and the scaling derived from H-mode database ($\tau_{E,92H}$), respectively. The open markers and the closed markers represent the H-mode database of KSTAR discharges ($\tau_{E,KSTAR,H}$) and the L-mode database of KSTAR discharges ($\tau_{E,KSTAR,L}$), respectively.

auxiliary heating sources which consist of up to ~3.0 MW power of NBI and up to ~0.4 MW power of 110 GHz ECRH. As absorbed power by ECRH is negligible compared with NBI due to its 2nd harmonic absorption at $B_T = 2.0$ T, NBI can be considered as the primary heating in most of discharges in the KSTAR database. Therefore, we only consider NBI for calculating the absorbed power by plasmas. The NBI power loss ($P_{NBI\ loss}$) consists of shine-through, charge exchange, and bad ion orbit as following;

$$P_{NBI\ loss} = P_{NBI\ shr} + P_{NBI\ CX} + P_{NBI\ Orbit}. \quad (2)$$

$P_{NBI\ loss}$ can be calculated by the NBI module [21] embedded in ASTRA [22] and NUBEAM [23]. The NBI module in ASTRA adopts a fluid approach, while NUBEAM the Monte Carlo description. Figure 2 shows $P_{NBI\ loss}$ due to shine-through, charge exchange, and bad ion orbit for some selected discharges with $P_{NBI} = 1.5$ MW where $P_{NBI\ shr}$ is calculated by the NBI module in ASTRA and $P_{NBI\ CX}$ and $P_{NBI\ Orbit}$ are calculated by NUBEAM. It is clearly seen that $P_{NBI\ shr}$ is less than 0.1 MW (<5% of P_L) and $P_{NBI\ CX}$ and $P_{NBI\ Orbit}$ are less than 0.02 MW (<1% of P_L). Furthermore, they are decreasing exponentially against $\bar{n}_e$ so their contribution to P_L can be negligible in the density range of the database. Therefore, we decide to exclude $P_{NBI\ loss}$ in estimating P_L in this work.

The measurement of the power of radiation (P_{rad}) has not been available in KSTAR experiments yet so that contribution of P_{rad} is also not considered in this analysis.

2.3. Multi-machine scalings selected for analysis of KSTAR discharges

The plasma stored energy is taken from the diamagnetic loop in calculation of $\tau_{E,KSTAR}$, which implies that $\tau_{E,KSTAR}$ calculated is not 'thermal' energy confinement time but 'global' energy confinement time. Because the density profiles are not available in the selected database for KSTAR, we can only deal with multi-machine scalings for global energy confinement. Thermal energy confinement analysis is limited, i.e. treating $\tau_{E,th}$ to subtract a contribution of fast ion energy ($W_{fast\ ion}$) driven by NBI from W_{dia} requires whole plasma kinetic profiles which could not be obtained routinely in KSTAR up to now. In addition, multi-machine scalings for P_L not considering P_{rad} can only be used since its measurement is not available in the KSTAR database.

Based on these criteria, we selected two multi-machine scalings to evaluate $\tau_{E,KSTAR}$ among various multi-machine scalings of τ_E for L- and H-modes established to extrapolate the energy confinement time of ITER as follows.

$$\tau_{E,89L} = 0.048 M_{eff}^{0.50} \kappa^{0.50} I_P^{0.85} \bar{n}_e^{0.10} B_T^{0.20} P_L^{-0.50} a^{0.30} R^{1.20} \quad (3)$$

$$\tau_{E,92H} = 0.021 M_{eff}^{0.50} \kappa^{0.70} I_P^{0.55} \bar{n}_e^{0.17} B_T^{0.91} P_L^{-0.55} R/a^{-0.19} R^{2.30} \quad (4)$$

In these scalings, M_{eff} represents an effective atomic mass in a plasma. $\tau_{E,89L}$ [4] represents a multi-machine scaling

based on the L-mode discharge database where the subscription 'L' indicates the L-mode scaling. $\tau_{E,92H}$ [7] represents a scaling based on the H-mode discharge database where the subscription 'H' implies the H-mode scaling.

3. Evaluation of global energy confinement against multi-machine scalings in KSTAR

3.1. Characteristics of KSTAR confinement against multi-machine scalings

Figure 3 shows $\tau_{E,KSTAR}$ against the scaling laws selected in the previous section where the confinement enhancement of KSTAR plasmas is evaluated in terms of H_{89L}, H_{89H}, H_{92L}, and H_{92H}. Here the notations of H_{89H} and H_{92H} are the confinement enhancement factor of 'H-mode database of KSTAR discharges' compared with the L- and H-mode multi-machine scalings, $\tau_{E,89L}$ and $\tau_{E,92H}$, respectively; $H_{89H} = \tau_{E,KSTAR,H}/\tau_{E,89L}$, $H_{92H} = \tau_{E,KSTAR,H}/\tau_{E,92H}$ where $\tau_{E,KSTAR,H}$ is the global energy confinement time of KSTAR H-modes. In a similar way, the notations of H_{89L} and H_{92L} are the confinement enhancement factor of 'L-mode database of KSTAR discharges' compared with the multi-machine scalings, $\tau_{E,89L}$ and $\tau_{E,92H}$, respectively; $H_{89L} = \tau_{E,KSTAR,L}/\tau_{E,89L}$, $H_{92L} = \tau_{E,KSTAR,L}/\tau_{E,92H}$ where $\tau_{E,KSTAR,L}$ is the global energy confinement time of KSTAR L-modes. In figure 3, the circle markers and the square markers represent $\tau_{E,KSTAR}$ against the scalings derived from L-mode database ($\tau_{E,89L}$) and the scaling derived from H-mode database ($\tau_{E,92H}$), respectively. The open markers and the closed markers represent the H-mode database of KSTAR discharges ($\tau_{E,KSTAR,H}$) and the L-mode database of KSTAR discharges ($\tau_{E,KSTAR,L}$), respectively. In the figure, $\tau_{E,KSTAR,L}$ takes place in the range from ~0.04 to ~0.16 s and $\tau_{E,KSTAR,H}$ from ~0.06 to ~0.19 s. Discharges exhibiting relatively low τ_E are due to relatively higher P_{aux}, mainly P_{NBI}.

In figure 3, H_{89H} (slope of open circle markers) is evaluated as ~1.4 to ~2.2. It implies that some KSTAR H-modes with $H_{89H} < 1.5$ exhibit rather worse confinement than standard H-modes ($H_{89H} \sim 2.0$) even close to the L-mode confinement ($H_{89H} \sim 1.0$) although the discharges are equipped with typical type-I ELMs. On the other hand H_{89L} (slope of closed circle markers) is observed to be ~0.9 to ~1.6 implying that some KSTAR L-modes with $H_{89L} > 1.5$ exhibit somewhat better confinement than standard L-modes ($H_{89L} \sim 1.0$) and even very close to the H-mode confinement ($H_{89L} \sim 2.0$). The similar trend is found with the $\tau_{E,92H}$ scaling. H_{92H} (slope of open squared markers) is evaluated as ~0.6 to ~1.2 and H_{92L} (slope of closed square markers) ~0.4 to ~0.7.

The standard deviations of H_{89H} and H_{92H} are 0.29 and 0.24, respectively which are relatively similar. Also the standard deviations of H_{89L} and H_{92L} are 0.24 and 0.09, respectively. It is interesting to note that the standard deviation of H_{92L} is the lowest for the KSTAR database even though $\tau_{E,92H}$ is the multi-machine scaling developed for the H-mode discharges.

Figure 4 shows H_{89H} corresponding to open circle markers in figure 3 which describes the characteristic of KSTAR H-mode confinement against $\tau_{E,89L}$ by isolating dependency

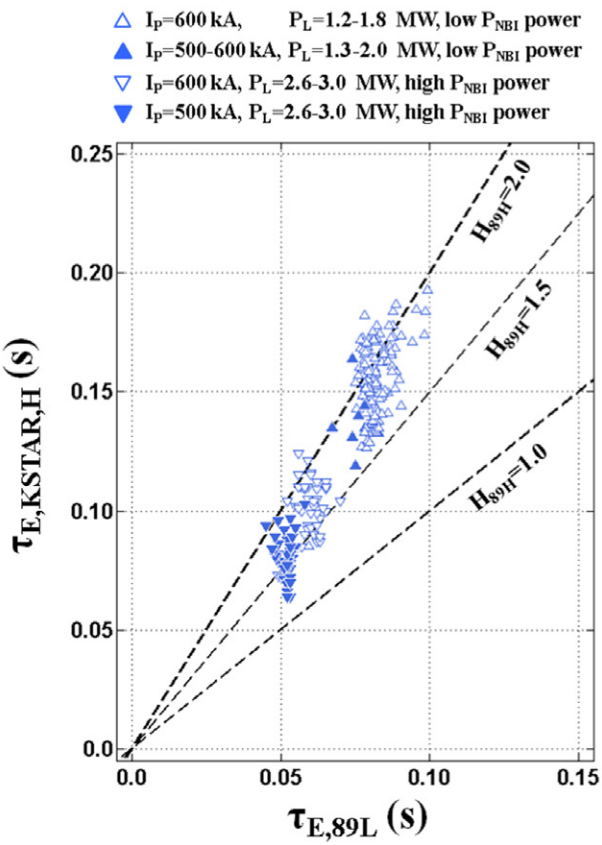

Figure 4. H_{89H} of KSTAR H-mode plasmas ($\tau_{E,KSTAR,H}$ versus $\tau_{E,89L}$ of KSTAR H-mode database). The open triangles and the closed triangles represent the case with low P_L and I_P of 600 kA and the case with low P_L and I_P of 500–600 kA, respectively. The open inverted triangles and the closed inverted triangles represent the case with high P_L and I_P of 600 kA and the case with high P_L and I_P of 500 kA, respectively.

of I_P and P_L. The open triangles and the closed triangles represent the case with low P_L and I_P of 600 kA and the case with low P_L and I_P of 500–600 kA, respectively. The open inverted triangles and the closed inverted triangles represent the case with high P_L and I_P of 600 kA and the case with high P_L and I_P of 500 kA, respectively. From figure 4, we can expect that $\tau_{E,KSTAR,H}$ exhibits a positive power component to I_P but a negative one to P_L, as $\tau_{E,89L}$ and $\tau_{E,92H}$ scalings do. Therefore, even though there are some deviations observed in the confinement enhancement factors based on the multi-machine scalings, KSTAR L- and H-mode discharges are regarded as following the basic trends appeared in the scalings.

3.2. Multiple regression analysis of global energy confinement time of KSTAR discharges

In order to derive an exact degree of influence of engineering parameters on $\tau_{E,KSTAR}$, a regression analysis is carried out for both L- and H-mode database in KSTAR. The multiple regression analysis is done by the IBM Statistical Package for the Social Sciences (SPSS) statistics. The ordinary least square method and the stepwise method are adopted to derive multiple regression equations. We choose the five variables as independent variables, i.e. I_P, B_T, P_L, κ, and $\bar{n}_e$. As

Table 2. The significance test of the driven multiple regression equation estimated with five independent predictors (I_P, B_T, $\bar{n}_e$, κ, P_L) for the L-mode database in KSTAR.

$\tau_{E,KSTAR,L}$ model	Included variables	Adjusted R^2	Std. error of the estimate	F	Sig.	Unstandardized coefficients	Standardized coefficients			Collinearity statistics	Excluded variables			Collinearity statistics
						B	β	t	Sig.	VIF		t	Sig.	VIF
1[a]		0.823	0.056	361.827	0.000									
	(Constant)					0.845		−83.671	0.000		I_P	22.711	0.000	
	P_L					−0.851	−0.908	−31.707	0.000	1.000	B_T	4.452	0.000	1.059
											$\bar{n}_e$	1.55	0.123	1.116
											κ	0.354	0.724	1.085
2[b]		0.948	0.031	1244.265	0.000									
	(Constant)					−0.561		−41.202	0.000		B_T	0.409	0.683	1.059
	P_L					−0.795	−0.848	−53.837	0.000	1.028	$\bar{n}_e$	1.943	0.053	1.116
	I_P					1.287	0.358	22.711	0.000	1.028	κ	−4.718	0.000	1.085
3[c]		0.953	0.029	921.275	0.000									
	(Constant)					−0.344		−7.205	0.000		B_T	1.279	0.202	1.116
	P_L					−0.814	−0.868	−55.624	0.000	1.109	$\bar{n}_e$	1.700	0.091	1.085
	I_P					1.345	0.374	24.265	0.000	1.082				
	κ					−0.757	−0.075	−4.718	0.000	1.156				

[a] Predictors: (Constant), P_L.
[b] Predictors: (Constant), P_L, I_P.
[c] Predictors: (Constant), P_L, I_P, B_T, κ.

Table 3. The significance test of the driven multiple regression equations estimated with five independent predictors (I_P, B_T, $\bar{n}_e$, κ, P_L) for the H-mode database in KSTAR.

$\tau_{E,KSTAR,H}$ model	Included variables	Adjusted R^2	Std. error of the estimate	F	Sig.	Unstandardized coefficients	Standardized coefficients			Collinearity statistics	Excluded variables			Collinearity statistics
						B	β	t	Sig.	VIF		t	Sig.	VIF
1[a]		0.593	0.075	361.827	0.000									
	(Constant)					−0.675		−50.486	0.000		I_P	23.384	0.000	
	P_L					−0.710	−0.771	−19.022	0.000	1.000	B_T	−0.475	0.635	1.059
											$\bar{n}_e$	6.187	0.000	1.116
											κ	1.284	0.200	1.085
2[b]		0.909	0.035	1244.265	0.000									
	(Constant)					−0.398		−35.029	0.000		B_T	−5.067	0.000	1.059
	P_L					−0.658	−0.714	−37.138	0.000	1.010	$\bar{n}_e$	1.255	0.211	1.116
	I_P					1.304	0.565	29.384	0.000	1.010	κ	−4.991	0.000	1.085
3[c]		0.918	0.034	921.275	0.000									
	(Constant)					−0.328		−18.663	0.000		$\bar{n}_e$	−1.125	0.262	1.116
	P_L					−0.664	−0.721	−39.234	0.000	1.017	κ	−6.956	0.000	1.085
	I_P					1.332	0.577	31.218	0.000	1.027				
	B_T					−0.218	−0.094	−5.067	0.000	1.025				
4[d]		0.931	0.031	836.704	0.000									
	(Constant)					−0.101		−2.798	0.006		$\bar{n}_e$	0.617	0.538	1.116
	P_L					−0.686	−0.745	−43.385	0.000	1.059				
	I_P					1.412	0.611	34.681	0.000	1.116				
	B_T					−0.285	−0.122	−7.016	0.000	1.085				
	κ					−0.684	−0.126	−6.956	0.000	1.175				

[a] Predictors: (Constant), P_L.
[b] Predictors: (Constant), P_L, I_P.
[c] Predictors: (Constant), P_L, I_P, B_T.
[d] Predictors: (Constant), P_L, I_P, B_T, κ.

mentioned in section 2.1, R and a are neglected here for two reasons; they are more or less invariant in the database and the regression is only for a single machine. The significance level is set to be 0.05 in the whole process of the regression. As the regression is preceded, any variable not satisfying the significance probability is removed by following the stepwise method. For this reason, $\bar{n}_e$ is removed in the regression process of the H-mode database. B_T as well as $\bar{n}_e$ are removed in the regression process of the L-mode database. That is, the removed variables do not contribute significantly in estimation of $\tau_{E,KSTAR}$ in statistical point of view. In tables 2 and 3, the whole set of evaluated scaling laws is presented which is estimated by the stepwise method. The regression adopted in this work which exhibits the best performance is presented in the last column. The multiple regression equations produced in this work are as follows:

$$\tau_{E,KSTAR,L,scaling} = 0.453\kappa^{-0.76\pm0.32} I_P^{1.35\pm0.11} P_L^{-0.81\pm0.03} \quad (5)$$

$$\tau_{E,KSTAR,H,scaling} = 0.793\kappa^{-0.68\pm0.20} I_P^{1.41\pm0.08} B_T^{-0.29\pm0.08} \times P_L^{-0.69\pm0.03} \quad (6)$$

Equations (5) and (6) are the empirical scalings driven on the basis of the L-mode database and the H-mode database in KSTAR, respectively.

They are evaluated in two ways. Firstly, the statistical significance is tested. In the KSTAR L-mode scaling (equation (5) and table 2), the adjusted R square is 0.953 and the F is 921.275 so that the p value (Sig.) corresponding F value is less than 0.05. Also, the p value of each independent variable corresponding t value is less than 0.05. In the KSTAR H-mode

scaling (equation (6) and table 3), the adjusted R square is 0.931 and the F-test and the t-test show the same sense as shown in equation (5). We can find out that the p values of all independent variables in the driven regression equations reach the values less than 0.05 so that the null hypothesis could be rejected. The summary of this significance test is presented in tables 2 and 3. Secondly, the multicollinearity is tested for equations (5) and (6). The variance inflation factors (VIFs) of κ, I_P, and P_L in equation (5) are 1.156, 1.082, and 1.109, respectively. The VIFs of κ, I_P, B_T, and P_L in equation (6) are 1.175, 1.116, 1.085, and 1.059, respectively. Hence we can draw a conclusion that there is hardly any correlation between the predictor variables. Therefore, the driven multiple regression equations and their entire estimated power components of independent variables achieve the confidence level and are significant statistically.

Now we try to compare the driven scalings with the multi-machine scalings. The L-mode scaling, $\tau_{E,KSTAR,L,scaling}$ and the H-mode scaling, $\tau_{E,KSTAR,H,scaling}$ can be directly compared with $\tau_{E,89L}$ and $\tau_{E,92H}$, respectively. The driven multiple regression equations exhibit the similar dependency on P_L in accord with figure 4, but higher dependency on I_P compared with the multi-machine scalings. The largest deviation comes from the dependency on κ. It exhibits opposite trends compared with the multi-machine scalings; highly negative in both driven scalings while positive in both multi-machine scalings. This is clearly seen in figure 5 which depicts dependency of $\tau_{E,KSTAR,H}$ and $\tau_{E,89L}$ on κ in the KSTAR H-mode database. Here, the data points are carefully selected having similar I_P and P_L, the same dataset shown as the closed inverted triangles in figure 4. As κ increases, $\tau_{E,KSTAR,H}$ decreases whereas $\tau_{E,89L}$ increases. Consequently, H_{89H} significantly deteriorates with κ. For this reason, the data points of the inverted triangles in figure 4 would take place more or less vertically by crossing slopes of $H_{89H} \sim 1.5$ and $H_{89H} \sim 2.0$ rather than lying on the slope of $H_{89H} \sim 2.0$. Although the origins of this abnormal trend are not confirmed yet, two possible candidates exist. One is concerned with the wall condition. The wall condition of KSTAR in the year 2012 was especially not good due to some events; a tile cracking at the first wall and a NBI operation fault occurred during the campaign. The other is related with the striking point control. The striking points on the divertor plate were uncontrolled in KSTAR experiments which made it difficult control impurity influxes to the plasma. As κ increases, not only the length from the X-point to the divertor plates becomes shortened but also the deposition of striking points on divertor plates becomes far more distant from the vacuum pump embedded in the divertor. So the impurities from the wall can penetrate into plasmas more easily resulting in confinement degradation. Details need to be figured out in the future.

In addition we attempt to derive the scaling laws for KSTAR with the same independent variables (seven variables, except M_{eff}) of the multi-machine scaling laws to compare directly with multi-machine scaling laws. In the statistical analysis, we extract a regression equation without excluding any variable among the seven even if a variable is not significant statistically against the significance level 0.05. The multiple regression equations derived with the seven predictors are

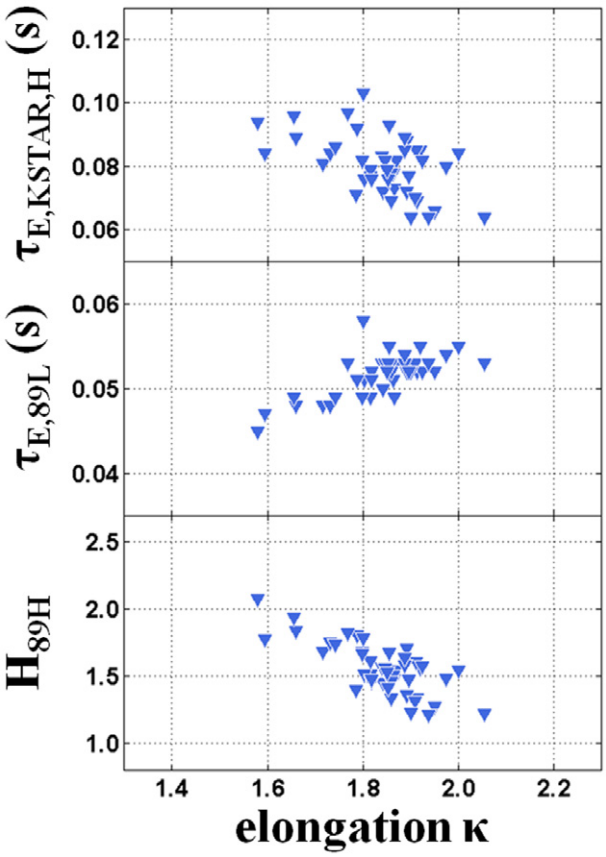

Figure 5. Dependency of $\tau_{E,KSTAR,H}$ and $\tau_{E,89L}$ on κ in the KSTAR H-mode database; (*a*) $\tau_{E,KSTAR,H}$, (*b*) $\tau_{E,89L}$, and (*c*) H_{89H}.

represented as follows:

$$\tau_{E,KSTAR,L,scaling} = 0.157\kappa^{-0.76\pm0.32} I_P^{1.35\pm0.12} \bar{n}_e^{0.07\pm0.05} \times B_T^{0.04\pm0.11} P_L^{-0.84\pm0.04} a^{-0.43\pm0.42} R^{1.17\pm1.12} \quad (7)$$

$$\tau_{E,KSTAR,H,scaling} = 0.383\kappa^{-0.82\pm0.21} I_P^{1.43\pm0.09} \bar{n}_e^{0.01\pm0.06} \times B_T^{-0.24\pm0.09} P_L^{-0.72\pm0.06} R/a^{-0.24\pm0.39} R^{1.87\pm1.07} \quad (8)$$

Equations (7) and (8) represent the L-mode and H-mode scaling law in KSTAR, respectively. As compared with the L-mode multi-machine scaling (equation (3)), the driven multiple regression equation of L-mode (equation (7)) has the similar dependency on $\bar{n}_e$ and R, but higher dependency on I_P and P_L, and lower dependency on B_T. Note that the variation of B_T has very weak influence on $\tau_{E,KSTAR,L}$ and the predictors a and κ have the opposite sign in comparison with $\tau_{E,89L}$. As compared with the H-mode multi-machine scaling (equation (4)), the driven multiple regression equation of H-mode (equation (8)) has the similar dependency on R/a, but higher dependency on I_P and P_L, and lower dependency on $\bar{n}_e$ and R. Note that the variation of $\bar{n}_e$ has little impact on $\tau_{E,KSTAR,H}$ and the independent variables B_T and κ exhibit the opposite sign in comparison with $\tau_{E,92H}$.

The results of the significant test are summarized in tables 4 and 5. From table 4, the sig. of B_T is 0.419 exceeding the assumed significance level which is the only one among all the independent variables. The VIFs of predictors in equation (7) are somewhat higher than those in equation (5), but they seem to present little correlation between them. In table 5,

Table 4. The significance test of the driven multiple regression equation estimated with seven independent predictors (I_P, B_T, $\bar{n}_e$, κ, P_L, R, a) for the L-mode database in KSTAR.

$\tau_{E,KSTAR,L}$ model	Included variables	Adjusted R^2	Std. error of the estimate	F	Sig.	Unstandardized coefficients	Standardized coefficients			Collinearity statistics
						B	β	t	Sig.	VIF
1[a]		0.954	0.029	647.904	0.000					
	(Constant)					−0.804		−4.519	0.000	
	P_L					−0.836	−0.891	−42.552	0.000	2.082
	I_P					1.349	0.375	22.415	0.000	1.328
	B_T					0.043	0.014	0.810	0.419	1.488
	κ					−0.763	−0.076	−4.763	0.000	1.201
	$\bar{n}_e$					0.070	0.051	3.024	0.003	1.345
	R					1.166	0.046	2.050	0.042	2.417
	a					−0.433	−0.035	−2.041	0.043	2.082

[a] Predictors: (Constant), P_L, I_P, B_T, κ, $\bar{n}_e$, R, a.

Table 5. The significance test of the driven multiple regression equation estimated with 7 independent predictors (I_P, B_T, $\bar{n}_e$, κ, P_L, R, R/a) for the H-mode database in KSTAR.

$\tau_{E,KSTAR,H}$ model	Included variables	Adjusted R^2	Std. error of the estimate	F	Sig.	Unstandardized coefficients	Standardized coefficients			Collinearity statistics
						B	β	t	Sig.	VIF
1[a]		0.934	0.030	498.956	0.000					
	(Constant)					−0.417		−3.642	0.000	
	P_L					−0.721	−0.783	−25.725	0.000	3.458
	I_P					1.430	0.619	31.216	0.000	1.470
	B_T					−0.244	−0.104	−5.451	0.000	1.370
	κ					−0.820	−0.151	−7.627	0.000	1.462
	$\bar{n}_e$					0.005	0.004	0.171	0.864	1.654
	R					1.868	0.103	3.435	0.001	3.382
	R/a					−0.239	−0.043	−1.219	0.224	4.598

[a] Predictors: (Constant), P_L, I_P, B_T, κ, $\bar{n}_e$, R, R/a.

the sig. of $\bar{n}_e$ and R/a are 0.864 and 0.224, respectively which exceed the assumed significance level. Although the VIFs of predictors in equation (8) are less than half of the reference point 10, but higher than those in equation (6). Therefore, the some predictors (e.g. P_L, R and R/a) in equation (8) could have multicollinearity compared with those in equation (6).

Lastly, it can be deduced which parameter makes a significant impact on the global energy confinement in KSTAR from the standardized coefficient in tables 2–5. Mostly P_L in L-mode plasma and P_L and I_P in H-mode plasma are influential factors exhibiting a strong correlation with the global energy confinement time.

4. Characteristics of KSTAR confinement in each discharge

Here, we revisit H_{exp} to evaluate how much plasma confinement is enhanced in the H-mode phase relative to the L-mode phase in a single discharge as made in early confinement analysis [11–13]. The analysis time points for calculating H_{exp} are the same as described in section 2.1. But we constrain ourselves to analyze discharges performed in FY 2012 only where the plasma control was conducted better than FY 2011.

Figure 6 represents $\tau_{E,KSTAR,H}$ versus $\tau_{E,KSTAR,L}$, i.e. H_{exp} ($=\tau_{E,KSTAR,H}/\tau_{E,KSTAR,L}$), in each discharge. H_{exp} is located mainly in the range from ∼1.3 to ∼2.4 as shown in figure 6. Some discharges located close to H_{exp} ∼ 1.3 are regarded as barely enhanced H-mode phases and some close to

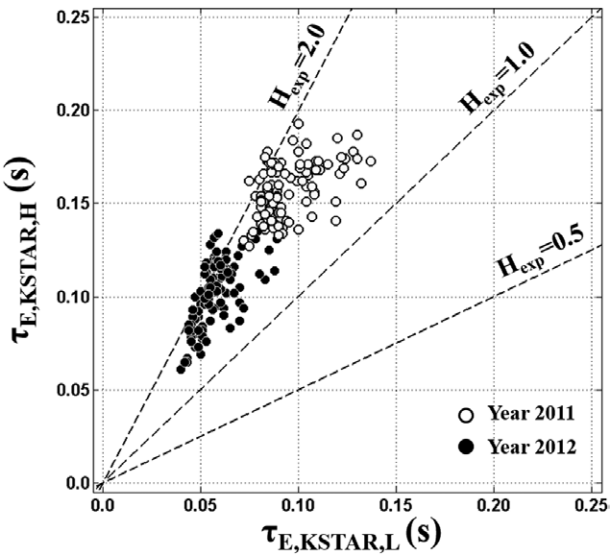

Figure 6. $\tau_{E,KSTAR,H}$ versus $\tau_{E,KSTAR,L}$, i.e. H_{exp} ($=\tau_{E,KSTAR,H}/\tau_{E,KSTAR,L}$), in each discharges. H_{exp} evaluates how much plasma confinement is enhanced as accessing the H-mode phase compared with the L-mode phase in each discharge within the database. The open markers represent the database in the year 2011 and the closed markers represent the database in the year 2012.

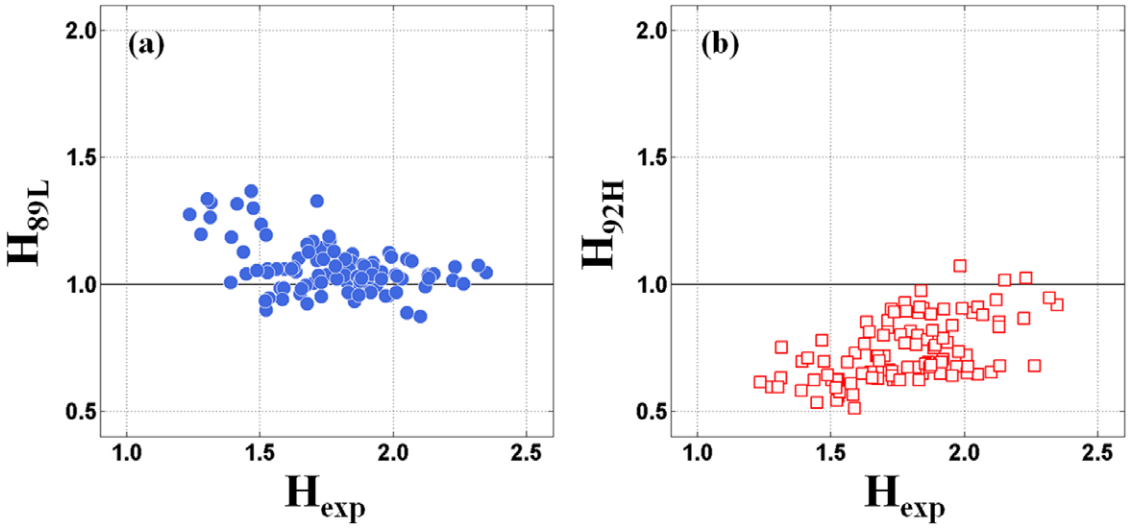

Figure 7. (*a*) $H_{89L}(=\tau_{E,KSTAR,L}/\tau_{E,89L})$ versus H_{exp} $(=\tau_{E,KSTAR,H}/\tau_{E,KSTAR,L})$ and (*b*) $H_{92H}(=\tau_{E,KSTAR,H}/\tau_{E,92H})$ versus H_{exp} $(=\tau_{E,KSTAR,H}/\tau_{E,KSTAR,L})$. By comparing them, one can identify that in what conditions the multi-machine scalings $\tau_{E,89L}$ and $\tau_{E,92H}$ work well in estimating $\tau_{E,KSTAR}$ of L- and H-mode phase in KSTAR, respectively.

$H_{exp} \sim 2.4$ are as highly enhanced H-mode phases compared with the L-mode phase of each discharge.

To compare this with the multi-machine scalings, figure 7 describes the relation between $H_{89L}(=\tau_{E,KSTAR,L}/\tau_{E,89L})$ and $H_{exp}(=\tau_{E,KSTAR,H}/\tau_{E,KSTAR,L})$ and the relation between $H_{92H}(=\tau_{E,KSTAR,H}/\tau_{E,92H})$ and $H_{exp}(=\tau_{E,KSTAR,H}/\tau_{E,KSTAR,L})$. By comparing them, one can identify that in what conditions the multi-machine scalings $\tau_{E,89L}$ and $\tau_{E,92H}$ agree with $\tau_{E,KSTAR}$ of L-mode and H-mode phase in KSTAR, respectively. In figure 7(*a*), as H_{exp} increases, $H_{89L}(=\tau_{E,KSTAR,L}/\tau_{E,89L})$ decreases and approaches unity. Therefore, if H_{exp} is large enough to be above 1.5, $\tau_{E,KSTAR,L}$ gets close to $\tau_{E,89L}$ so that one can say that $\tau_{E,89L}$ can estimate $\tau_{E,KSTAR,L}$ well. In a similar fashion, as H_{exp} increases, $H_{92H}(=\tau_{E,KSTAR,H}/\tau_{E,92H})$ increases and approaches unity as shown in figure 7(*b*). Therefore, if H_{exp} is large enough above $\sim$2.0, $\tau_{E,KSTAR,H}$ gets close to $\tau_{E,92H}$ so that one can say that $\tau_{E,92H}$ can estimate $\tau_{E,KSTAR,H}$ well. Nevertheless, $\tau_{E,92H}$ cannot fit $\tau_{E,KSTAR,H}$ as accurate as $\tau_{E,89L}$ can fit $\tau_{E,KSTAR,L}$. One can expect that if $\tau_{E,KSTAR,H}$ is more enhanced compared with $\tau_{E,KSTAR,L}$, (higher H_{exp} than that has been achieved so far), the multi-machine scaling $\tau_{E,92H}$ can estimate $\tau_{E,KSTAR,H}$ better. It is interesting to note that not only $\tau_{E,KSTAR,L}$ is higher than $\tau_{E,89L}$ but also $\tau_{E,KSTAR,H}$ is lower than $\tau_{E,92H}$ for discharges with insufficient confinement enhancement of the H-mode phase than the L-mode phase in a single discharge ($H_{exp} < 1.5$) as shown in figure 7. Although we have investigated the physics behind in terms of engineering parameters, no rigorous conclusion has been made yet for this phenomenon. We expect more systematic analysis such as transport modeling can be possible if all the kinetic profiles are available in the near future. H_{exp} are also compared with $H_{89H}(=\tau_{E,KSTAR,H}/\tau_{E,89L})$. H_{exp} has the same physical meaning with H_{89H} of the confinement enhancement of H-mode over L-mode plasmas. We recall that H_{89H} in KSTAR presents in the range of $\sim$1.3 to $\sim$2.3 which exhibits a similar of H_{exp} as mentioned above. H_{89H} is compared with H_{exp} in figure 8(*a*). At a first glance, H_{89H} looks accord closely with H_{exp}. However, if one looks into in more detail, H_{89H} is observed to be higher than H_{exp} for discharges with low H_{exp} but lower for discharges with high H_{exp}. This becomes clear if introducing R_H defined as the ratio between H_{exp} and H_{89H}, i.e. $R_H = H_{89H}/H_{exp}$ which is depicted in figure 8(*b*). In the region of $\sim 1.5 < H_{exp} <\sim 2.0$, the difference between H_{exp} and H_{89H} is small implying that H_{89H} works. However, H_{89H} is almost $\sim$1.3 times bigger than H_{exp} at maximum as H_{exp} decreases down to $H_{exp} \sim 1.3$. That is, even though the confinement of the H-mode phase is not much enhanced against the L-mode phase for discharges with $H_{exp} <\sim 1.5$, the H-mode phase can be evaluated to be highly enhanced and overestimated when using the $\tau_{E,89L}$ scaling. On the contrary, even though the confinement of the H-mode phase is highly enhanced against the L-mode phase for discharges with $H_{exp} >\sim 2.0$, the H-mode phase can be evaluated to be less enhanced and underestimated about 20% when using the $\tau_{E,89L}$ scaling.

In addition, it is worthy to notify that the H-mode phase of KSTAR discharges in the range of $H_{exp} <\sim 1.5$ cannot be evaluated properly by both L- and H-mode multi-machine scalings ($\tau_{E,89L}$ and $\tau_{E,92H}$). The H-mode phase with $H_{exp} <\sim 1.5$ is evaluated not only to be less enhanced when using the H-mode multi-machine scaling ($\tau_{E,92H}$) as shown in figure 7(*b*) but also to be highly enhanced when using the L-mode multi-machine scaling ($\tau_{E,89L}$) as shown in figure 8(*b*). It is obvious that the data points located in $H_{exp} <\sim 1.5$ cannot be explained by the multi-machine scalings.

5. Conclusion

We evaluate the characteristics of global energy confinement of about 250 discharges in KSTAR discharges both in the L- and the H-mode phase collected for two years (from the year 2011 to the year 2012). Firstly, the global energy confinement time is calculated and compared with multi-machine scalings. Secondly, the multiple regression equation for the L- and the H-mode, respectively is derived and

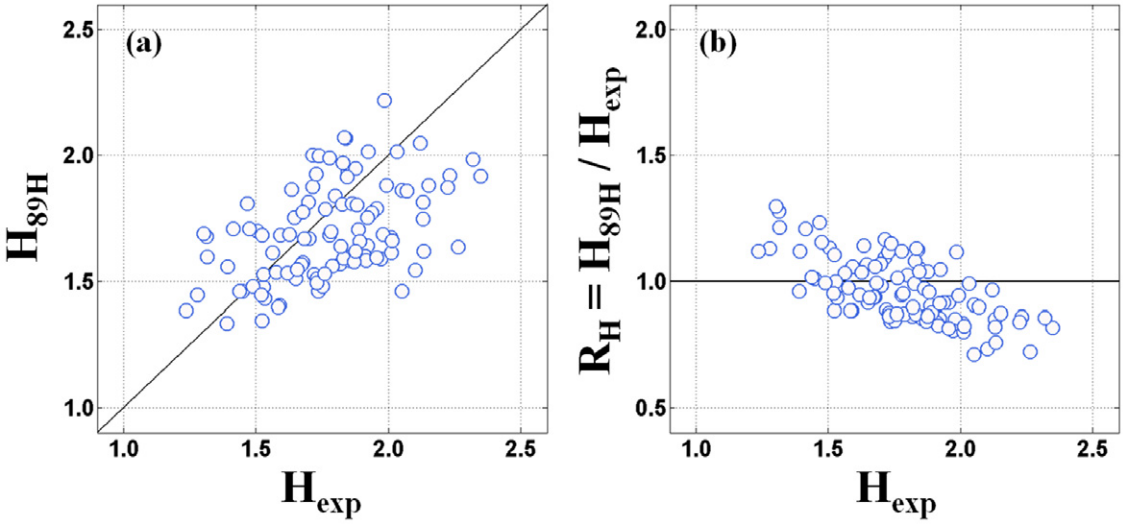

Figure 8. (*a*) H_{exp} versus $H_{89H}(=\tau_{E,KSTAR,H}/\tau_{E,89L})$ and (*b*) H_{exp} versus $R_H(=H_{89H}/H_{exp})$. This figure describes how much the actual confinement enhancement of KSTAR discharges differs from one predicted by the multi-machine scalings, $\tau_{E,89L}$.

compared with multi-machine scalings. Lastly, confinement enhancement of the H-mode phase with respect to the L-mode phase is evaluated in each discharge. In the KSTAR database, $\tau_{E,KSTAR,L}$ is calculated to be in the range of ~0.04 to ~0.16 s and $\tau_{E,KSTAR,H}$ in ~0.06 to ~0.19 s. In terms of confinement enhancement factors, H_{89H} and H_{92H} yield from ~1.4 to ~2.2 and from ~0.6 to ~1.2, respectively in the KSTAR H-mode database. H_{89L} and H_{92L} are in the range of ~0.9 to ~1.6 and ~0.4 to ~0.7, respectively in the KSTAR L-mode database. Even though there are some deviations in the confinement enhancement factors based on the multi-machine scalings observed, KSTAR is shown to follow the basic trend of the multi-machine scalings. The multiple regression equations are derived by statistical analysis for $\tau_{E,KSTAR,H}$ and the $\tau_{E,KSTAR,L}$, which exhibit the similar dependency on P_L but higher dependency on I_P compared with the multi-machine scalings. Interestingly, the dependency on κ in both $\tau_{E,KSTAR,H,scaling}$ and $\tau_{E,KSTAR,L,scaling}$ is revealed to be highly negative apart from the positive behaviour in multi-machine scalings. Although the reason is not clear yet, two possibilities are addressed. One is that the wall condition of KSTAR was not clean enough. The other is that striking points on the divertor plate were uncontrolled. For these reasons, as κ increases, the impurities from the wall are supposed to penetrate into plasmas more easily. As a consequence, the confinement is degraded on the contrary to the expectation of multi-machine scalings. H_{exp} $(=\tau_{E,KSTAR,H}/\tau_{E,KSTAR,L})$ is applied to evaluate the characteristics of $\tau_{E,KSTAR}$ in each discharge. It has been found that if H_{exp} is large enough, $\tau_{E,KSTAR,L}$ looks to follow the multi-machine L-mode scaling, $\tau_{E,89L}$. In a similar fashion, if H_{exp} is large enough, $\tau_{E,KSTAR,H}$ looks to follow the multi-machine H-mode scaling $\tau_{E,92H}$. Therefore, we can conclude that the energy confinement of both L- and H-mode of the KSTAR discharges with $H_{exp} > 1.5$ can be well-predicted by multi-machine scalings $\tau_{E,89L}$ and $\tau_{E,92H}$ for L-mode and for H-mode, respectively. Apart from this, the H-mode confinement with $1.5 < H_{exp} < 2.0$ is well-predicted by using the multi-machine empirical L-mode scaling $\tau_{E,89L}$. On the other hand, the H-mode confinement with $H_{exp} < 1.5$ cannot be estimated properly by both the L-mode scaling $\tau_{E,89L}$ and the H-mode scaling $\tau_{E,92H}$. In our work, the characteristics of global energy confinement in KSTAR plasmas are evaluated quantitatively. We expect that the extrapolation to next step devices such as ITER is envisaged with updated database from forthcoming KSTAR experiment.

Acknowledgments

This research was supported by National R&D Program through the National Research Foundation of Korea (NRF) funded by the Ministry of Science, ICT & Future Planning (No. 2013036099) and the R&D Program through the National Fusion Research Institute of Korea (NFRI) funded by the Government funds.

References

[1] Yushmanov P.N. 1990 *et al Nucl. Fusion* **30** 1999
[2] Kaye S.M. *et al* 1985 *Nucl. Fusion* **25** 65
[3] Kaye S.M. *et al* 1990 *Phys. Fluids* B **2** 2926
[4] Christiansen J.P. *et al* 1992 *Nucl. Fusion* **32** 291
[5] Schissel D.P. 1993 H-Mode Database Working Group presented at *Proc. 20th Eur. Conf. on Controlled Fusion Plasma Physics (Lisbon, Portugal, 1993)* vol 17C, Part 1 (Geneva: European Physical Society) pp 103
[6] Kardaun O. 1992 H-Mode Database Working Group *Proc. 14th Int. Conf. on Plasma Physics and Controlled Nuclear Fusion Research (Würzburg, Germany, 1993)* vol 3 (Vienna: IAEA) p 251 www-naweb.iaea.org/napc/physics/FEC/STIPUB906_VOL3.pdf
[7] ITER H Mode Database Working Group 1994 *Nucl. Fusion* **34** 131
[8] Miura Y. *et al* 1992 *Nucl. Fusion* **32** 1473
[9] Cordey J.G.; ITER Confinement Database and Modeling Working Group 1997 *Plasma Phys. Control. Fusion* **39** B115
[10] ITER Physics Expert Groups in Confinement and Transport 1999 ITER Physics Basis: chapter 2. Plasma confinement and transport *Nucl. Fusion* **39** 2175

[11] Wagner F. *et al* 1982 *Phys. Rev. Lett.* **49** 1408
[12] Keilhacker M. *et al* 1986 *Plasma Phys. Control. Fusion* **28** 29
[13] Ohyabu N. *et al* 1985 *Nucl. Fusion* **25** 49
[14] Lee G.S. *et al* 2000 *Nucl. Fusion* **40** 575
[15] Kwon M. *et al* 2011 *Nucl. Fusion* **51** 094006
[16] Yoon S.W. *et al* 2011 *Nucl. Fusion* **51** 113009
[17] Park Y.S. *et al* 2013 *Nucl. Fusion* **53** 083029
[18] Byun C.-s. *et al* 2014 *Current Appl. Phys.* **14** 144
[19] ITER Confinement Modelling and Database Group 1998 ITER Profile Database, Standard list of variables and file format http://tokamak-profiledb.ccfe.ac.uk/DOCS/Manual_may_98.pdf
[20] Ejima S. *et al* 1982 *Nucl. Fusion* **22** 1313
[21] Polevoi A. *et al* 1997 JAERI-Data/Code 97-014, Japan Atomic Energy Research Institute www.iaea.org/inis/collection/NCLCollectionStore/_Public/28/052/28052091.pdf
[22] Pereverzev G.V. *et al* 2002 *IPP Report* 5/98 Max-Planck Institut fur Plasmaphysik www.pppl.gov/∼hammelt/work/2009/Astra_ocr.pdf
[23] Pankin A. *et al* 2004 *Comput. Phys. Commun.* **159** 157